Direct visualization of colloidal gelation under confinement

Prasad S. Sarangapani,[1] Yanghai Yu,[1] Jiang Zhao,[2] and Yingxi Zhu[1]
[1]*Department of Chemical and Biomolecular Engineering, University of Notre Dame, Notre Dame, Indiana 46556, USA*
[2]*Institute of Chemistry, Chinese Academy of Sciences, Beijing, China 100080*
(Received 14 January 2008; published 30 June 2008)

The physical mechanism of colloidal gelation remains inadequately understood, particularly for intermediate to high volume fractions. Experiments to directly probe the complex evolution of structural and viscoelastic properties of gels have been few despite their fundamental importance in elucidating the physical mechanisms responsible for gelation. In this study, we use a home-built micron-gap rheometer combined with confocal microscopy to directly investigate the coupled structural and dynamic properties of colloidal gelation transition by spatial confinement. We observe that confinement-induced gelation proceeds by a spinodal decomposition route where strongly confined colloidal suspensions evolve into "colloid-rich" and "colloid-poor" regions; the propagation of the "colloid-rich" region in three dimensions is responsible for structural arrest and strong viscoelastic enhancement when a critical film thickness approaches 16–25 particle layers.

DOI: 10.1103/PhysRevE.77.061406 PACS number(s): 82.70.Gg, 64.70.pv, 83.10.Tv, 68.18.Jk

I. INTRODUCTION

Gels are a class of cross-linked amorphous materials characterized by a tenuous, fractal network of polymeric clusters [1]. Particles in the colloidal domain can aggregate to form a physical gel by either tuning the interparticle interaction or applying external forces to the system. Distinct from the physical gel that is often reversible is the chemical gel, where polymeric chains branch out to form interconnected clusters by covalent bonds, thereby resulting in an often irreversible gel network [1]. The properties of a gel, formed by either a physical or chemical process, are rather intriguing: Despite its tenuous open network, the elastic modulus of a gel is finite [1] and highly dependent on the bonding strength among colloidal clusters [2], which is crucial for controlling rheological properties of soft materials for their broad technological applications ranging from surface coatings to drug delivery. Though many experimental and theoretical studies have endeavored to probe the physical underpinnings of a fluid-gel transition by studying model physical gels formed from colloidal particle aggregates [2–13], few have succeeded in capturing the complex evolution of the coupled structural, dynamic, and viscoelastic properties near the gelation point.

The most general mechanism for colloidal gelation in dilute suspensions is diffusion limited cluster aggregation (DLCA) [4], where colloidal particles in a suspension collide by virtue of their Brownian motion and aggregate in the presence of attractive interparticle interactions to form large clusters with a wide distribution of length scales that grow until divergence, resulting in the formation of a nonergodic gel. However, generalizing colloidal gelation processes under DLCA neglects many subtle properties of gelation; structural and dynamic features of gels are rather diverse due to their strong dependence on interparticle interaction and volume fraction. Manley *et al.* [3] demonstrate that a subtle yet strong connection between gelation and the glass transition exists at moderate volume fractions, where gelation is driven by spinodal decomposition into a "colloid-poor" region and a "colloid-rich" interconnected network and the relaxation time for particles in the "colloid-rich" region is on the same order of magnitude as a hard-sphere suspension close to the colloidal glass transition. Mechanistic investigations into dynamic properties of depletion-induced colloidal gels from intermediate to high volume fractions by Gao and Kilfoil [5] also show the signature of dynamic heterogeneity: Separable fast and slow populations are identified where the slow populations consist of a space-spanning "backbone" of particles analogous to the force chains found in granular media as well as the rigid, percolating slow clusters in hard-sphere colloidal glasses [14,15]. Atomistic simulations have also contributed to a greater understanding of the details of gelation, where Puertas *et al.* have analyzed dynamical heterogeneity in depletion gels [6]. Motivated by these experimental and computational studies, theorists have largely explored gelation using the mode coupling theory (MCT) of supercooled liquids [7,16], considering that the slow relaxation dynamics in supercooled liquids is analogous to gels whose structural relaxation can span several decades in time. The naive MCT [8,17] also predicts the colloidal sol-gel transition in depletion gels and their elastic moduli with a strong dependence on the radius of gyration of the nonadsorbing polymer, polymer concentration as well as particle volume fraction, which are in good agreement with experimental results [9]. However, the naive version of MCT [8,17] mainly works for hard-sphere colloidal suspensions with low volume fraction and weak attraction, where kinetically driven structural arrest is expected, but fails to capture the essence of colloidal gelation under strong interparticle attraction and/or at intermediate to high volume fraction via multiple pathways that include percolation, network collapse, and so on.

Accompanied with the formation of a space-spanning network as the gelation point approaches is the abrupt change in the viscoelastic properties from a liquidlike state to a solidlike state upon gel formation. However, the determination of the gelation point often relies on the sudden change of either structural or viscoelastic properties as volume fraction increases. In this work, we employ an alternative experimental approach by using spatial confinement between two solid substrates to directly probe the evolution a fluid-gel transi-

tion in colloidal suspensions, where a dimensional reduction impedes structural relaxation and results in the formation of a space-spanning gel network. We use a microgel system, poly-*N*-(isopropylacrylamide) (PNIPAM) particles suspended in aqueous media, which has been much investigated due to its intriguing thermo-responsive and *p*H-responsive features with potential applications for sensing and therapeutic applications [10]. PNIPAM microgel particles, inside which polymerized NIPAM chains are chemically crossed linked and stable, can further interact to form a thermoreversible physical gel without hysteresis [11]. Previous work has indicated that nonergodicity upon a gelation transition strongly depends on the pathways, but not intrinsically on chemical cross-linking [12]. In this work, we use a custom-built micron-gap rheometer interfaced with an inverted confocal microscope to simultaneously explore the coupling of the film thickness dependent phase structure, single-particle dynamics and rheological properties of PNIPAM microgel suspensions confined between two solid surfaces. To the best of our knowledge, it is the first time that direct structural visualization combined with the *in situ* measurement of viscoelastic properties near the gelation point is experimentally conducted with confined colloidal thin films. We surmise from our observations that confinement-induced gelation is largely driven by the separation of the suspension into "colloid-rich" and "colloid-poor" regions, where the "colloid-rich" region shows strong viscoelastic enhancement and is glasslike in nature and the propagation of the "colloid-rich" region drives structural arrest.

II. EXPERIMENTAL

Sample preparation and characterization. PNIPAM microgel is synthesized using the method of emulsion polymerization described elsewhere [18,19]. An aqueous solution of fluorescein disodium at a concentration of 1×10^{-4} M is added into the resulting suspension in a 1:10 volume ratio to dye PNIPAM microgel particles. The resultant suspension is then dialyzed for two weeks at room temperature using a SpectraPor® dialysis membrane with a diameter of 20.4 mm and flat width of 32 mm and redispersed in fresh deionized water before experiments.

Dynamic light scattering-based particle size analyzer (Brookhaven ZetaPALS) and confocal laser scanning microscopy (CLSM) (Zeiss LSM 5 Pascal) are employed to determine the particle diameter, polydispersity, and phase structure of synthesized PNIPAM particles suspended in deionized water, as shown in the inset of Fig. 1. The diameter measured by the particle size analyzer and confirmed by CLSM is 1.6 μm with a polydispersity of 7%. The particles are fully swollen at room temperature, suggesting that the solvent quality is "good" [10,18]. Additionally, the van der Waals attractions between particles are minimized as the microgel particles contain approximately 97% water thus the refractive indices of the microgel particles and water are essentially the same. To verify the thermo-responsive behavior of the synthesized PNIPAM microgel, we also characterize the temperature dependence of fluorescent PNIPAM particle size by using a heating/cooling stage (INSTEC) mounted on the sample stage of inverted CLSM. As shown in Fig. 1, the particle diameter decreases approximately 50% as temperature approaches 32–34 °C, in good agreement with its lower critical solubility temperature (LCST) reported in the literature [10,12].

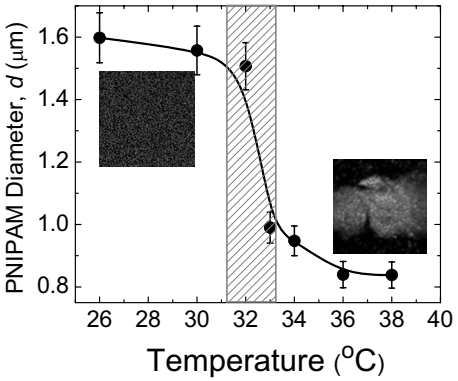

FIG. 1. PNIPAM microgel diameter as a function of temperature. The lower critical solubility temperature (LCST) is identified as highlighted in the shaded area. Inset: a representative fluorescent micrograph showing the 2D structure of PNIPAM in the bulk aqueous suspension below the LCST ($T=25$ °C) and above the LCST ($T=37$ °C), respectively.

Experimental setup and data analysis. A home-built micron-gap rheometer (MGR) is employed to study the structural and dynamic properties of confined PNIPAM thin films of varied thickness in a sphere-flat plate geometry using two optical-smooth quartz surfaces. As shown by the schematic diagram in Fig. 2, the MGR is mounted on the sample stage of the inverted Zeiss CLSM to allow three-dimensional visualization of confined PNIPAM microgel particles through an oil-immersion objective lens ($NA=1.4$, 63×).

Colloidal PNIPAM suspensions are stirred vigorously overnight before pipetting the suspension into a sample chamber sealed with high vacuum grease to mitigate evaporation. The suspension is confined between a spherical smooth quartz disk and a smooth flat quartz surface (ESCO) and in contact with a large reservoir of bulk suspension. The sample is equilibrated for ~30 min to let transient flow dis-

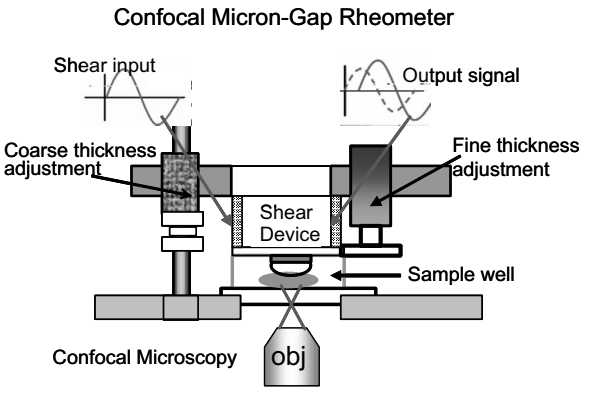

FIG. 2. Schematic diagram of the custom-designed micron-gap rheometer (MGR) that is mounted on the stage of an inverted confocal microscope.

sipate before measurements. To vary film thickness of confined PNIPAM microgel suspensions, we systematically decrease film thickness step-wise by using a high-precision micrometer (Newport) at a compression rate of $\sim 10\ \mu m/min$ with an additional 5 min interval between each compression step to minimize mechanical drift. When the desired film thickness is reached, we wait an additional 20 min before data acquisition to minimize hydrodynamic effects. Film thickness is determined by both the readings of micrometer and confocal z-stack profile with an accuracy of $\pm 0.2\ \mu m$. All experiments are conducted at a constant temperature, $T=25\pm 0.1\ ^\circ C$.

The design of the MGR using a pair of piezoelectric bimorphs is described elsewhere [20,21]. To probe the viscoelastic properties of confined microgel thin films, sinusoidal shear forces of input amplitude A_0 are applied to one piezoelectric bimorph, the resulting thin-film displacement is detected by a second bimorph and a lock-in amplifier (Stanford Research Systems, SR850) is used to decompose the measured response into output amplitude A and phase lag. The response of confined thin films measured in terms of amplitude attenuation A_0/A and phase shift θ are analyzed to determine the spring constant k and dashpot coefficient ωb of colloidal suspension (L), confined between two surfaces, as $k_L=K_{sp}(A_0 \cos \theta/A\text{-}1)$ and $\omega b_L=K_{sp}A_0 \sin \theta/A$, where K_{sp} is the effective spring constant of the rheometry assembly and calibrated from the bulk viscoelastic properties of microgel suspensions by using a strain-controlled rheometer (Rheometrics) in a parallel-plate geometry. The elastic G' and viscous G'' moduli of microgel thin films are obtained as $G'=(H/A_C)k_L$ and $G''=(H/A_C)\omega b_L$, respectively [20,21], where H is the film thickness and A_C is the contact area, both determined microscopically [17,18]. The measured bulk moduli of PNIPAM suspension (see Fig. 4) are used to determine K_{sp} ($\sim 4900\ N/m$) for the data analysis of confined PNIPAM thin-film viscoelasticity.

During the experiment, suspension microstructure and particle mobility are simultaneously visualized and recorded using the CLSM over a typical x-y scanning area of $78 \times 78\ \mu m^2$ at a resolution of 512×512 pixels^2. Wall effects are mitigated by acquiring images several particles layers away from the confining substrates.

Image analysis. Particle centroid-finding algorithms [22] are employed to identify particle positions and obtain trajectories for approximately 1000 particles for all images acquired in time series. We identify particle positions with a resolution of $0.05\ \mu m$ in the x-y plane and of $0.1\ \mu m$ in the z direction. A PNIPAM aqueous suspension of bulk particle volume fraction $\phi=0.18$ is prepared in this work. The effective particle volume fraction of confined PNIPAM thin films is computed by counting the number n of fluorescent particles present in the viewing volume V of confocal micrographs via centroid finding algorithms and calculated as $\phi=\pi d^3 n/6V$, where d is the particle diameter.

III. RESULTS AND DISCUSSION

We start our analysis by considering the formation and propagation of a space-spanning gel under confinement as shown in the confocal micrographs in Fig. 3. We focus on the confinement-induced clustering of PNIPAM microgel thin films. We visualize and analyze the suspension microstructure at least six particle layers from each confining substrate to mitigate wall effects. Figure 3(a) shows a liquidlike equilibrium sol with virtually no gelation in the bulk suspension of $\phi=0.18$, indicating no long-range spatially correlated clusters. Upon decreasing film thickness to $H/d=25$, we observe a ramified interconnected cluster network that is separated from a low-density fluid phase as shown in Fig. 3(b),

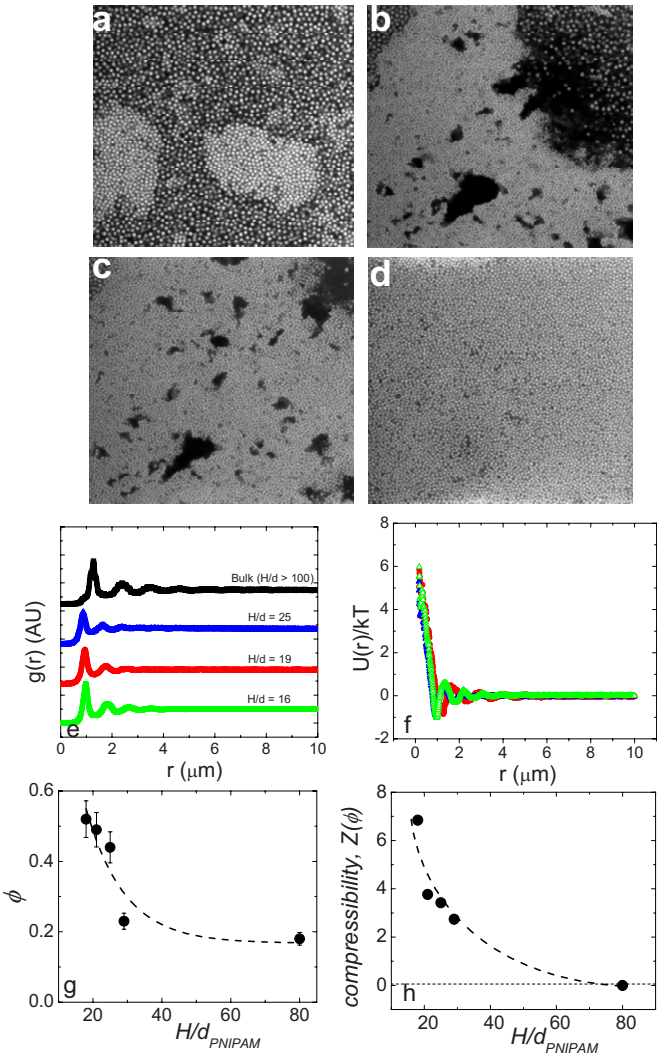

FIG. 3. (Color online) Fluorescent micrographs of PNIPAM suspensions show the formation of PNIPAM clusters and a space-spanning gel under confinement. (a) The bulk PNIPAM suspension showing an equilibrium sol virtually without gelation. (b) Confinement-induced clustering with spinodal decomposition evident at normalized film thickness H by particle diameter d, $H/d=25$. (c) Formation of a more continuous, kinetically arrested gel phase with fewer fluid voids at $H/d=19$. (d) Space-spanning structure with kinetically arrested PNIPAM particles at $H/d=16$. (e) Pair correlation function for the bulk (black squares), $H/d=25$ (red circles), 19 (blue upper triangles), and 16 (green down triangles). (f) Corresponding interaction potential at varied film thickness H/d. (g) Measured volume fraction plotted against normalized film thickness, H/d. (h) Compressibility factor Z plotted against H/d.

suggesting the emergence of a space-spanning gel structure. This picture is consistent with a mechanism of spinodal decomposition as the driving force for gelation proposed from recent experimental observation with colloidal depletion gels [3]. Further reduction in film thickness to $H/d=19$ results in the formation of a more continuous "colloid-rich" phase with fewer fluid voids as shown in Fig. 3(c), suggesting the emergence of a gel-to-glass transition provided with the divergence in cluster correlation length R_c within the "colloid-rich" phase as $R_c \sim d\phi^{1/(d_f-3)}/2$, where d_f is the fractal dimension. Indeed, a gel-to-glass transition is confirmed at lesser film thickness $H/d=16$, where a continuous, kinetically arrested phase is evident in Fig. 3(d), where particles appear trapped in cages formed by their neighbors. The fractal dimension, d_f increases from $d_f=1.91$ for the bulk to $d_f=1.99$ for $H/d=16$, suggesting that the gel structure has tiled the two-dimensional phase space.

Gelation in the bulk [13] is often governed by varying the interparticle interaction, such as enhancing depletion through the addition of nonadsorbing polymer and reducing electrostatic repulsion through the addition of salt to aqueous suspensions. Our PNIPAM system could be best approximated as a system of "soft spheres," where the weak interparticle attraction is possibly due to hydrophobic attraction [18] between the hydrophobic blocks on PNIPAM chains and van der Waals attraction when the microgel particles are in close contact. To examine how the depth of the potential well changes with film thickness, we estimate entropic interaction potential of mean force [in Fig. 3(f)] from the pair correlation function [in Fig. 3(e)] using the relation $g(r)=\exp[-U(r)/kT]$ [22]. The pair correlation functions shown in Fig. 3(e) for different gaps show rather convincingly, that the phase behavior we have observed for our system differs significantly from previous studies of PNIPAM microgel, which have found that the phase behavior of PNIPAM microgel closely resembles hard-spheres, where fluid-crystal coexistence is usually observed for volume fractions of $\phi \sim 0.5$. The absence of crystallization in our system for similar volume fractions examined in Ref. [5], indicate the uniqueness of the system we have considered. It is evident that the minima in the interaction potential shifts to lower r, indicating the attractive potential well is more short-ranged with decreasing film thickness. However, in our case, colloidal gelation under confinement is accompanied by the increase in the three-dimensional particle volume fraction of PNIPAM microgel thin films, which is analyzed from z-stack confocal micrographs and shown in Fig. 3(g), leading to the possible compaction of PNIPAM aggregate structure. To examine this effect, we compute the compressibility factor Z of PNIPAM microgel clusters at varied film thickness as $Z=(\nu_p/\phi k_B T)\Pi(\phi)$, where ν_p is the particle volume as $\nu_p=\pi d^3/6$ and $\Pi(\phi)$ is the ϕ-dependent osmotic pressure obtained from a direct numerical integration of the volume fraction profile across film thickness $\Pi(\phi)=\Delta\rho g\int_0^H \phi(z)dz$ [23], where $\Delta\rho$ is the density difference between the PNIPAM microgel particle and water, H is the measured film thickness, and g is the gravitational constant. The calculated osmotic pressure ranges from 0.02 Pa for the bulk suspension to 0.12 Pa for confined PNIPAM thin film of $H/d=16$, which suggests that the increase in external compression to reduce film thickness can effectively result in the formation of clusters as well as the propagation of a ramified, space-spanning cluster network under strong confinement. As shown in Fig. 3(h), the compressibility factor Z of PNIPAM microgel thin films increases rapidly with decreasing film thickness. It should be noted that the compressibility factor we obtain ($Z\sim 7$) for a volume fraction of $\phi=0.5$ is less than the value of hard-spheres [23]. This deviation from hard-sphere behavior could be associated with attractions among particles. Moreover, we conjecture that the abrupt increase of the compressibility factor, taken together with the fractal dimensions reported above, is related to a divergent cluster correlation length R_c under confinement where a percolation threshold has been reached [24], giving rise to a sharp increase in the compressibility factor as the critical film thickness approaches $H/d \leq 25$.

To explore the correlations between structural and viscoelastic properties of confined microgel thin films, we examine their viscoelastic response in the bulk and under confinement near the gelation point. Considering the coupling of film thickness and volume fraction of confined PNIPAM thin films as discussed above, we use a traditional strain-controlled rheometer to first examine the linear viscoelasticity of bulk PNIPAM suspensions at corresponding volume fractions $\phi=0.18-0.51$ as shown Fig. 4(a). Linear response up to a strain rate $\gamma=40\%$ at a fixed frequency of $\omega=10$ rad/s is verified for the bulk PNIPAM microgel suspension for all volume fractions up to $\phi=0.51$. Due to the sensitivity limitation of the rheometer used in this work, we can only obtain the frequency-dependent linear shear spectrum at $\gamma=40\%$ for bulk PNIPAM microgel suspension at $\phi=0.30$ and 0.51. The elastic moduli G' for both volume fractions dominates over the viscous moduli G'' over the entire range of frequency sweeps and is weakly dependent on frequency, reflecting the elastic nature of a gel phase formed at intermediate to high volume fractions. The viscous and elastic moduli for bulk PNIPAM suspensions are also used to calibrate our micron-gap rheometer to ensure that the moduli of bulk suspensions measured by two different rheometers are comparable. As the bulk rheology data indicate that the measured G' greatly exceeds G'' over the frequency sweep range at $\phi=0.30-0.51$, we now focus on the thickness dependence of elastic moduli G' of confined PNIPAM microgel thin films as shown in Fig. 4(b). It is very striking to observe that for strongly confined PNIPAM suspensions ranging from $H/d=16-25$, the measured elastic moduli increase dramatically with decreasing film thickness and are $4\sim 5$ orders of magnitude higher than the bulk value even for the bulk at highest $\phi=0.51$ examined in this work. For the confined thin films at $H/d=16-25$, the measured elastic moduli approximately scale with frequency ω with a power law $G' \sim \omega^{0.5}$ at low frequency, suggesting the typical viscoelastic behavior of "soft glassy materials" [25,26]; at high frequency, the plateau in G' is a typical response in the "glass zone" for many viscoelastic materials due to insufficient time for structural relaxation, suggesting the onset of structural arrest of strongly confined PNIPAM particles [27].

The viscoelastic properties of the PNIPAM suspensions inferred from the bulk and micron-gap rheological measurements are ensemble averaged and do not capture the complex

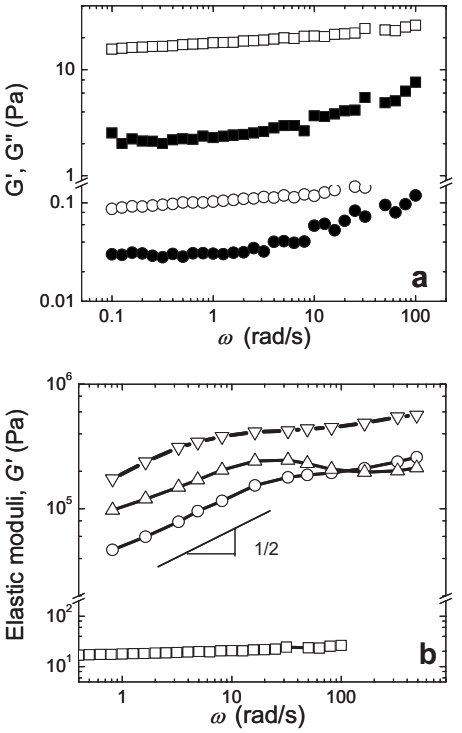

FIG. 4. (a) Linear frequency-dependent shear spectra of bulk PNIPAM suspensions at $\phi=0.30$ (squares), $\phi=0.51$ (circles). Elastic moduli G' (open symbols) and viscous moduli G'' (filled symbols) are measured at a fixed strain amplitude $\gamma=40\%$ and a fixed frequency of $\omega=10$ rad/s by using a strain-controlled rheometer in a parallel-plate geometry. (b) Measured frequency-dependent elastic modulis G' for confined PNIPAM suspensions at $H/d=25$ (circles), $H/d=19$ (upper triangles), $H/d=16$ (down triangles) at $\gamma=40\%$, in comparison to the elastic moluli for the bulk PNIPAM suspension at $\phi=0.51$ (squares). Below $\omega=10$ rad/s, G' scales with radian frequency in a power law of 1/2, and above $\omega=15$ rad/s, G' exhibits a very weak frequency dependence.

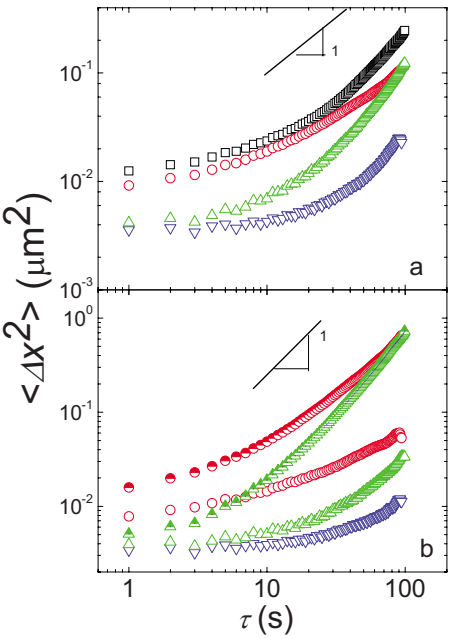

FIG. 5. (Color online) Mean-square displacements (MSD) of confined PNIPAM suspensions for the bulk (squares), $H/d=25$ (circles), 19 (upper triangles), and 16 (down triangles). (b) Separate "fast" (semifilled symbols) and "slow" (open symbols) populations chosen by rank-ordering the particle displacements and choosing the 5% most mobile and immobile populations.

microscopic structural and dynamical features close to the gelation point. To investigate the dynamical properties in "colloid-rich" and "colloid-poor" regions we examine the particle mobility quantified in terms of the mean-square displacement (MSD) as

$$\langle \Delta x^2 \rangle = \frac{1}{N} \sum_{j=1}^{N} \langle [x_j(0) - x_j(\tau)]^2 \rangle \tag{1}$$

which is averaged over all particles in the scanning area and initial lag times τ along the x coordinate [28,29]. We focus on the 2D situation by analyzing the MSD along the x coordinate, parallel to the confining surfaces. Figure 5(a) shows the computed $\langle \Delta x^2 \rangle$ ensemble-averaged over all the particles in the scanning area as a function of τ at varied film thickness. It should be noted that the MSD along the x and y directions are essentially the same. We find that confinement induced slow dynamics is evident where the plateau in the MSD consistently decreases with film thickness, suggesting that particle motion becomes more localized and the long-time diffusivity is concomitantly reduced. Considering the contrast in PNIPAM particle mobility between "colloid-rich" and "colloid-poor" regions, we further quantify the distribution of fast and slow populations: In order to determine the distribution of fast and slow populations for the ensemble averaged MSD, we rank order the displacements $\Delta x_i(\tau)$ of individual particles and select the 5% of the most mobile and immobile particles [4] and plot the respective MSDs for each population in Fig. 5(b). Distinguishable fast and slow populations are indeed apparent for confined PNIPAM particles at $H/d=16-25$, where the appearance of a kinetically arrested "colloid-rich" region is separated from a fully ergodic "colloid-poor" region. Such heterogeneous dynamics that strongly depends on structural heterogeneity is in stark contrast to the behavior of hard-sphere colloidal suspensions approaching a glass transition and further suggests that spinodal decomposition is the driving force for gelation. It is intriguing to see that separable populations are no longer detected at $H/d=16$; instead, we find a space-spanning homogeneous kinetically arrested gel, which appears "glass-like."

While confinement results in the formation of a space-spanning gel network, it is of interest to examine how a growing amorphous "order" contributes to the slowing down of dynamics. To further investigate how the formation of a space-spanning gel cluster alters structural relaxation, we examine the overlap order parameter $q(\tau)$ [30]. This particular correlation function measures the number of "overlapping" particles separated by a distance a compared within a given time interval τ. The overlap order parameter is defined as

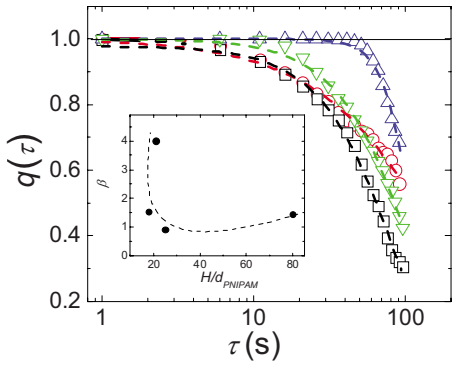

FIG. 6. (Color online) The overlap order parameter $q(\tau)$ for PNIPAM suspensions. The decay is increasingly stretched as film thickness decreases from the bulk ($H/d>100$) (squares) to $H/d=25$ (circles) until compressed exponential relaxation sets in at $H/d=19$ (upper triangles) and $H/d=16$ (down triangles) due to short range ballistic structural rearrangement. Inset: The Kolrausch exponent β which is obtained by fitting the curves shown in the main panel using the Kolrausch-Williams-Watts formula, is plotted against H/d.

$$q(\tau) = (1/N)\sum_{i=1}^{N} w[|r_i(0) - r_i(\tau)|] \tag{2}$$

where $w=1$ or 0 if $|r_i(0)-r_i(\tau)|$ is greater or less than the vibration amplitude of the particle a_{vib} estimated from the MSD using the Lindemann rule [31]. We choose this particular correlation function because of its high sensitivity to the evolution of slow dynamics, which is particularly important for the gel formation where the propagation of an amorphous, space-spanning network governs dynamical arrest. In this work, the length scale $a_{\mathrm{vib}}=0.13$ is chosen in correspondence to the vibration amplitude of the bulk sample, which is extracted from the inflection point in the MSD shown in Fig. 5(a), where a transition from transient caging to diffusive behavior is observed. Figure 6 shows the strong dependence of $q(\tau)$ on film thickness. Previous experimental investigations of gels [32] have shown anomalous scaling of the Kolrausch exponent, where β has been reported to exceed the unity. To examine the presence of compressed exponential decay, we fit all curves using the Kolrausch-Williams-Watts formula $q(\tau)=\exp[-(t/\tau)^{\beta}]$. For the bulk sample, we see nearly exponential decay with a Kolrausch exponent of $\beta=0.98$ which is expected for the equilibrium sol. Upon further decreasing film thickness we see in the Inset of Fig. 6 that the evolution of compressed exponential grows from $\beta=1.45$ to 4 for $H/d=25$ and 16, respectively, suggesting the approaching of a gelation point upon reducing film thickness. Additionally, the temporal correlation shows time invariance at short times compared to the bulk sol until a rapid decorrelation is observed. These results are intriguing and are consistent with Kolrausch exponents and scaling previously observed for multilamellar vesicles [33] and a model Lennard-Jones gel system studied by Del Gado and Kob [34]. Compressed exponential decay is usually attributed to ballistic stress induced rearrangements within the gel network. These ballistic rearrangements due to the applied stress are often attributed to highly mobile particles at the periphery of the gel structure which are diffusing into and away from the network. As a result, structural rearrangement occurs to accommodate the imposed stress to the "colloid-rich" gel network.

IV. CONCLUSION

In this paper, we have investigated the structural, viscoelastic, as well as single-particle dynamic properties of confined PNIPAM microgel suspensions by simultaneous structural visualization and dynamic measurements. Surprisingly, our results show an apparent gelation transition at a critical film thickness of $H/d=25$ where a space-spanning gel is formed and results in structural arrest, even though the PNIPAM microgel are well described by the "hard-sphere" phase diagram below their LCST. We observe scaling behavior in both the ensemble-averaged thin film rheology as well as the MSD. Viscoelastic enhancement is evident where the elastic modulus increases dramatically as film thickness is reduced; it is accompanied by a corresponding decrease in the MSD where PNIPAM particles remain strongly localized at lesser thickness. The overlap order parameter also demonstrates that confinement results in an increase in amorphous "order" as film thickness reduces. This is reflected in the longer correlation time and increased Kolrausch exponent at lesser thickness, demonstrating that the scaling is consistent with other systems that also display a gelation transition [1–4]. Taken together, all of the above observations lend credence to the picture that a general mechanism of spinodal decomposition might be responsible for gelation at intermediate to high volume fractions.

ACKNOWLEDGMENTS

We are indebted to Professor Davide A. Hill for assistance with the bulk rheology measurements. The authors are grateful for the financial support from the U.S. Department of Energy, Division of Materials Science (Grant No. DE-FG02-07ER46390) and the National Science Foundation (Grants No. CBET-0651408 and No. CBET-0730813).

[1] R. Larson, *Structure and Rheology of Complex Fluids* (Oxford University Press, New York, 1999).

[2] T. Gisler, R. C. Ball, and D. A. Weitz, Phys. Rev. Lett. **82**, 1064 (1999).

[3] S. Manley, H. M. Wyss, K. Miyazaki, J. C. Conrad, V. Trappe, L. J. Kaufman, D. R. Reichman, and D. A. Weitz, Phys. Rev. Lett. **95**, 238302 (2005).

[4] D. A. Weitz, J. S. Huang, M. Y. Lin, and J. Sung, Phys. Rev.

Lett. **53**, 1657 (1984).
[5] Y. Gao and M. L. Kilfoil, Phys. Rev. Lett. **99**, 078301 (2007).
[6] A. M. Puertas, M. Fuchs, and M. E. Cates, J. Phys. Chem. B **109**, 6666 (2005).
[7] K. A. Dawson *et al.*, Phys. Rev. E **63**, 011401 (2001); B. Ahlstrom and J. Bergenholtz, J. Phys.: Condens. Matter **19**, 036102 (2007); J. Bergenholtz, W. Poon, and M. Fuchs, Langmuir **19**, 4493 (2003); J. Bergenholtz and M. Fuchs, Phys. Rev. E **59**, 5706 (1999).
[8] Y.-L. Chen, V. Kobelev, and K. S. Schweizer, Phys. Rev. E **71**, 041405 (2005).
[9] S. Ramakrishnan and C. F. Zukoski, Langmuir **22**, 7833 (2006).
[10] J. Wu, B. Zhou, and Z. Hu, Phys. Rev. Lett. **90**, 048304 (2003); J. Wu, G. Huang, and Z. Hu, Macromolecules **36**, 440 (2003).
[11] Y. Zhao *et al.*, Macromolecules **36**, 855 (2003).
[12] B. R. Saunders and B. Vincent, Adv. Colloid Interface Sci. **80**, 1 (1999).
[13] S. Manley, J. M. Skotheim, L. Mahadevan, and D. A. Weitz, Phys. Rev. Lett. **94**, 218302 (2005).
[14] W. K. Kegel and A. van Blaaderen, Science **287**, 290 (2000).
[15] J. C. Conrad, P. P. Dhillon, E. R. Weeks, D. R. Reichman, and D. A. Weitz, Phys. Rev. Lett. **97**, 265701 (2006).
[16] T. Franosch and W. Gotze, J. Phys. Chem. B **103**, 4011 (1999).
[17] E. J. Saltzman and K. S. Schweizer, Phys. Rev. E **74**, 061501 (2006).
[18] Z. Hu and X. Xia, Adv. Math. **16**, 305 (2004).
[19] See EPAPS Document No. E-PLEEE8-77-117806 for the detailed experimental procedure. For more information on EPAPS, see http://www.aip.org/pubservs/epaps.html
[20] Y. Zhu and S. Granick, Phys. Rev. Lett. **87**, 096104 (2001).
[21] J. Peachey, J. Van Alsten, and S. Granick, Rev. Sci. Instrum. **62**, 463 (1991).
[22] J. C. Crocker and D. G. Grier, J. Colloid Interface Sci. **179**, 298 (1996).
[23] S. Buzzaccaro, R. Rusconi, and R. Piazza, Phys. Rev. Lett. **99**, 098301 (2007).
[24] A. de Candia *et al.*, Physica A **358**, 239 (2005).
[25] P. Sollich, F. Lequeux, P. Hébraud, and M. E. Cates, Phys. Rev. Lett. **78**, 2020 (1997).
[26] D. Bonn, S. Tanase, B. Abou, H. Tanaka, and J. Meunier, Phys. Rev. Lett. **89**, 015701 (2002).
[27] J. D. Ferry, *Viscoelastic Properties of Polymers* (Wiley, New York, 1980).
[28] E. R. Weeks and D. A. Weitz, Phys. Rev. Lett. **89**, 095704 (2002).
[29] P. S. Sarangapani and Y. Zhu, Phys. Rev. E **77**, 010501(R) (2008).
[30] A. S. Keys *et al.*, Nat. Phys. **3**, 260 (2007).
[31] F. H. Stillinger, Science **267**, 1935 (1995).
[32] A. Duri and L. Cipelletti, Europhys. Lett. **76**, 972 (2006).
[33] L. Ramos and L. Cipelletti, Phys. Rev. Lett. **87**, 245503 (2001).
[34] E. Del Gado and W. Kob, Phys. Rev. Lett. **98**, 028303 (2007).